Hindawi
Journal of Control Science and Engineering
Volume 2020, Article ID 4048507, 13 pages
https://doi.org/10.1155/2020/4048507

Research Article

Adaptive Super-Twisting Sliding Mode Control for Mobile Robots Based on High-Gain Observers

Haitao Liu,[1,2] **Jianhao Nie**,[1] **Jian Sun**,[1] **and Xuehong Tian**[1]

[1]*School of Mechanical and Power Engineering, Guangdong Ocean University, Zhanjiang 524088, China*
[2]*Southern Marine Science and Engineering Guangdong Laboratory (Zhanjiang), Zhanjiang 524000, China*

Correspondence should be addressed to Jianhao Nie; gdniejh@163.com and Xuehong Tian; gdtianxh@126.com

Received 29 October 2019; Revised 28 May 2020; Accepted 29 June 2020; Published 1 August 2020

Academic Editor: Carlos-Andrés García

In this paper, a robust adaptive output feedback control strategy based on a sliding mode super-twisting algorithm is designed for the trajectory tracking control of a wheeled mobile robot. First, a robust adaptive law is designed to eliminate the influence of parameter uncertainties. Second, a double-power sliding mode surface is designed to improve the response speed of the robot system. Finally, a high-gain observer is employed to estimate the speed information. The stability of the closed-loop system is proved using the Lyapunov stability theorem. The effectiveness of the proposed control strategy is verified by simulation.

1. Introduction

As a kind of practical operating tools, mobile robots have far-reaching application prospects in various industries. Mobile robots are highly nonlinear, continuous time-varying, strongly coupled dynamic systems. Therefore, it is an extremely challenging task to realize that mobile robots can overcome different external disturbances and track a predetermined trajectory in dissimilar environments. The parameters of their motion control system must be adjusted with the changes of the tracking path and the surrounding environment at all times to meet the requirements of precise control.

Nevertheless, through the unremitting efforts of researchers, the robust adaptive control method [1–3], sliding mode control method [4–7], and intelligent control method [8–10] have been used in the nonlinear control of mobile robots. These methods have their own advantages and disadvantages.

Although the traditional PID control has the characteristics of a simple principle, few parameters, and easiness of use, it has been extensively used in industrial process control. However, it is a linear combination of the three items of error proportional, integral, and derivative action, and it does not possess the function of adjusting gain parameters online. Therefore, traditional PID control is very limited to the tracking control of the complex nonlinear system signals such as mobile robots. With in-depth research of mobile robots by researchers, sliding mode control (SMC) technology has become a mature trajectory tracking control method for mobile robots. Sliding mode control has a lot of advantages, such as fast response and strong robustness to disturbances and system uncertainties. However, the main problem with this sliding mode method is the inevitable chattering phenomenon, which may harm the actuator. There are numerous techniques to reduce chattering, such as using the saturation function or the sigmoid function instead of the discrete control function [11, 12]. Although this approach reduces chattering, the robustness is weakened. If the parameter uncertainties change, characteristics such as finite-time convergence and robustness cannot be achieved, and steady-state error may occur. Another method to reduce chattering is used by second-order or high-order sliding mode control, such as the super-twisting algorithm. This method allows the finite-time convergence of sliding variables and their primary derivatives under disturbances and parameter uncertainties. In [6, 13–15], a second-order SMC based on the super-twisting algorithm was adopted. Compared with SMC, chattering is slightly reduced, and the robustness of the controller is maintained. Intelligent

control methods, such as neural network and fuzzy control, have been widely used in recent years. In [16], by using Artificial Neural Network (ANN) to obtain the decision-making ability of mobile robot speed control, the mobile robot can track and follow a target under any condition. Boukens et al. [17] employed adaptive neural networks to approximate mobile robot system uncertainties, and mechanical and electrical dynamics disturbances. In [18], a novel backstepping fuzzy sliding mode controller is presented for trajectory tracking control of wheeled mobile robot in the presence of model uncertainty and external interference. Wu and Karkoub [19] studied the trajectory tracking of a differential driven mobile robot with uncertainty and unknown dynamics using a hierarchical fuzzy sliding mode adaptive controller. The intelligent control algorithm does not rely on a mathematical model and provides a new means to solve the trajectory tracking control problem of mobile robots. However, the application of mobile robots still lacks technical support. Because of its complex control algorithm and large number of computations, it will occupy many system resources and directly affect real-time performance, which is an important requirement of mobile robot systems.

To achieve the purpose of output feedback for the control system, the observer is employed in mobile robots. Ovalle et al. [20] proposed four continuous sliding mode control strategies. In order to get an output feedback controller, a high-order sliding mode observer is implemented for each output signal. In [21], online state estimation sliding mode controller based on an adaptive super-twisting observer is proposed and applied to the positioning of the satellite system. However, the most widely utilized observers are high-gain observers. A motivating second-order example is utilized to illustrate the key features of high-gain observers and their use in feedback control [22]. Liu and Khalil [23] deduced the conditions for high-gain observer to achieve super-twisting control and compared the simulation of high-gain observer with sliding mode observer. Simulation results demonstrate that the performance of the two observers is equivalent, but the high-gain observer has a simple structure and is easier to implement in engineering. The implementation of a super-twisting control algorithm for a high-gain observer in an n^{th}-order perturbed integral system is introduced in [24]. In the literature [25, 26], some improvements have been done in the high-gain observer to improve the performance of the observer.

It is worth noting that a controller based on output feedback control is not common in mobile robot systems. It is also noteworthy that, in the study of mobile robot control strategies, most of the literature is based on three-wheel mobile robots. However, driving in real life, using four wheels is more conducive to keep the balance and stability of the robot. Therefore, this paper is intended to design the controller to achieve precise control of the four-omnidirectional-wheel mobile robots. To some extent, this article is inspired by study in [20, 23]. Compared with the literature [20], the improved control strategy improves the robustness of the system to external disturbances and makes the system respond faster. More importantly, the accuracy of trajectory tracking is significantly improved. The contributions of this article are as follows:

(1) In practical application, the use of a speed sensor to obtain the speed signal of the mobile robot makes its measurement accuracy vulnerable to the interference of climate and environment. Therefore, to prevent the use of high-cost speed sensors, a high-gain observer is designed to estimate the speed signal of the autonomous mobile robot effectively in real time, and the output feedback control of the system is achieved.

(2) Double-power sliding mode surface is designed to effectively speed up the convergence of the system.

(3) Uncertain parameters are considered, and a robust adaptive law that improves the robustness and trajectory tracking accuracy of the system is intended to fit the uncertain parameter.

(4) The resulting trajectory tracking error is very small, and the error level is approximately 10^{-6}, which is a startling trajectory tracking accuracy, although it is difficult to achieve this control accuracy in practical applications due to the influence of coupling terms between mechanical and electrical systems.

The structure of the article is as follows: the model description of the mobile robots is introduced in Section 2; the design of the high-gain observer is given in Section 3; the design step of the super-twisting sliding mode controller is described in detail in Section 4; the simulation results are provided in Section 5; and some conclusions are given in Section 6. Finally, the proofs of some theorems are provided in the appendix.

2. Model Description

In this paper, the omnidirectional mobile robot driven by four wheels is taken as the research object. The driving wheel adopted is the Mecanum wheel. The Mecanum wheel is compact and flexible, and it is a very lucrative omnidirectional wheel. It has been extensively employed in engineering applications. When the wheel rotates in a 45° arrangement, the free roller is connected to the ground, and the ground will create a 45° friction force between the wheel and the rotating shaft clip. The friction force can be split into the X component and the Y component. By changing the directions of the X and Y component forces by forward or reverse rotation or stopping the wheel, the platform can move in various ways, and its structure diagram is shown in Figure 1. The coordinate conversion relationship from the robot coordinate system cx_cy_c to the world coordinate system OXY is expressed as follows:

$$R(\theta) = \begin{bmatrix} \sin(\theta) & \cos(\theta) & 0 \\ -\cos(\theta) & \sin(\theta) & 0 \\ 0 & 0 & 1 \end{bmatrix}. \tag{1}$$

The dynamic equation of the omnidirectional mobile robot is described in [20] considering the actuator as follows:

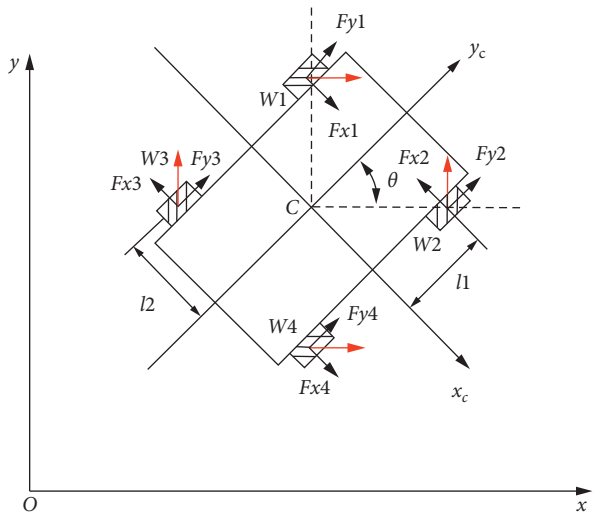

Figure 1: Structure diagram of the mobile robot.

$$M\ddot{q} + C(\dot{q})\dot{q} + D\dot{q} = \tau + \delta, \tag{2}$$

where M is the inertia matrix of the system; the elements on the diagonal are defined as $\mathrm{diag}\{M_1 \quad M_2 \quad M_3\}$; $q = [\,x \quad y \quad \theta\,]^T$ represents the pose of the mobile robot; $C(\dot{q})$ is the matrix of concentric force and Coriander force; D is a matrix related to motor parameters; $\tau = [\,\tau_1 \quad \tau_2 \quad \tau_3\,]^T$ is a vector of generalized forces; δ is the bounded disturbance vector; and $M, C(\dot{q}), D \in R^{3\times 3}$ are separately given by the following:

$$\begin{aligned} M &= M_C + \left(I + J_m r_e^2\right) EE^T, \\ C(\dot{q}) &= \frac{4}{r^2}\left(I + J_m r_e^2\right)\dot{\theta}B, \\ D &= r_e^2\left(\frac{k_a k_b}{R_a} + k_v\right)EE^T, \end{aligned} \tag{3}$$

where

$$\begin{aligned} M_C &= \begin{bmatrix} m_1 + 4m_2 & 0 & 0 \\ 0 & m_1 + 4m_2 & 0 \\ 0 & 0 & 4m_2\left(l_1^2 + l_2^2\right) + J_1 + 4J_3 \end{bmatrix}, \\ E &= \frac{1}{r}\begin{bmatrix} 1 & -1 & -(l_1 + l_2) \\ 1 & 1 & (l_1 + l_2) \\ 1 & -1 & (l_1 + l_2) \\ 1 & 1 & -(l_1 + l_2) \end{bmatrix}, \\ B &= \begin{bmatrix} 0 & 1 & 0 \\ -1 & 0 & 0 \\ 0 & 0 & 0 \end{bmatrix}, \end{aligned} \tag{4}$$

where m_1 is the mass of the robot body; m_2 is the mass of each wheel of the mobile robot; J_1 is the moment of inertia of the robot; J_2 is the moment of inertia of the wheel on the motor shaft; J_3 is the moment of inertia of the wheel in the vertical direction of the motor shaft; I is the unit inertia matrix; r_e is the transmission ratio; R_a is the armature resistance; k_a is the torque constant; k_b is the reverse EMF constant; k_v is the viscous friction coefficient of the motor; J_m is the moment of inertia of the motor shaft; r is the radius of the wheel; l_1 is half the length of the robot; l_2 is half the width of the robot; E is the reversal of the Jacobian matrix of the system; and B is a matrix.

We represent model (2) in state space, considering the changes in the following variables: $q = q_p = [\,x \quad y \quad \theta\,]^T$, $q_v = [\,\dot{x} \quad \dot{y} \quad \dot{\theta}\,]^T$. As a consequence, the state-space representation of model (2) is

$$\begin{bmatrix} \dot{q}_p \\ \dot{q}_v \end{bmatrix} = \begin{bmatrix} q_v \\ f(q_v) + G(\tau + \delta) \end{bmatrix}, \tag{5}$$

where $f(q_v)$ and G are expressed as follows:

$$f(q_v) = -M^{-1}[C(q_v) + D]q_v, \tag{6}$$

$$G = \mathrm{diag}\{M_1^{-1} \quad M_2^{-1} \quad M_3^{-1}\} \tag{7}$$

For the sake of convenience, G is converted to $G = \mathrm{diag}\{g_1 \quad g_2 \quad g_3\}$.

3. Design of Observer

In practice, it is difficult to directly measure the speed signal of a mobile robot owing to complex environmental interference. To avoid the use of high-cost velocity sensors, this paper uses separate principles to design the observer and controller separately. This chapter designs a high-gain observer for real-time estimation of the speed signal of the mobile robot during operation and realizes the output feedback control of the system.

The high-gain observer is designed as follows:

$$\begin{bmatrix} \dot{\hat{q}}_{pi} \\ \dot{\hat{q}}_{vi} \end{bmatrix} = \begin{bmatrix} \hat{q}_{vi} + \dfrac{\alpha_1}{\varepsilon}e_{pi} \\ \dfrac{\alpha_2}{\varepsilon^2}e_{pi} + f_i(\hat{q}_v) + g_i\tau_i \end{bmatrix}, \tag{8}$$

where $i = 1, 2, 3; \alpha_1, \alpha_2 > 0; 0 < \varepsilon < 1; \hat{q}_{pi}$ is the estimated value of the observation of the position; and $\hat{q}_{vi}$ is an estimated observation of the velocity. The position observation error is expressed as $e_{pi} = q_{pi} - \hat{q}_{pi}$.

Let $\phi = f_i(q_v) + g_i\tau_i$, and let $\phi_0 = f_i(\hat{q}_v) + g_i\tau_i$ be a nominal model of ϕ.

Remark 1. For the convenience of expression, we define the following symbolic rules: $[x]^\varphi = |x|^\varphi \mathrm{sign}(x)$.

Assumption 1. For any choice of ϕ_0, there are nonnegative constants L and M such that the following formula holds in the study area:

$$\left|\phi_0(z,u)-\phi(q,u)\right| \le L\|q-z\| + M. \tag{9}$$

For the particular case in which $\phi_0 = \phi$, if ϕ is uniform Lipschitz for q and u, then the above inequality holds, and $M = 0$.

Remark 2. Let $h_1 = (\alpha_1/\varepsilon), h_2 = (\alpha_2/\varepsilon^2)$, and $H = \mathrm{col}(h_1, h_2)$. The observation error $\tilde{q} = q - \hat{q}$ satisfies the following equation:

$$\dot{\tilde{q}} = A_0\tilde{q} + B_0\delta(q,\tilde{q},u), \tag{10}$$

where $A_0 = \begin{bmatrix} -h_1 & 1 \\ -h_2 & 0 \end{bmatrix}$, $B_0 = \begin{bmatrix} 0 \\ 1 \end{bmatrix}$, and $\delta(q,\tilde{q},u) = \phi_0(q,u) - \phi(\hat{q},u)$.

Assumption 2. There is a known normal number $\eta_i > 0\,(i = 1,2,3)$ satisfying the following conditions [20]:

$$\left|\frac{\mathrm{d}}{\mathrm{d}t}\tilde{\delta}_i\right| \le \eta_i, \tag{11}$$

where $\tilde{\delta}_i = g_i\delta_i + \tilde{f}_i$ and $\tilde{f}_i = f_i(q_v) - f_i(\hat{q}_v)$.

We define the observer estimation error of velocity state quantity as $e_{vi} = q_{vi} - \hat{q}_{vi}$. The observation error can be written as $e_i = \begin{bmatrix} e_{pi} & e_{vi} \end{bmatrix}^T$.

Theorem 1. *If the observer given in (6) is applied in system (2) and satisfies $H = col(h_1, h_2)$ such that A_0 is Hurwitz, then the observation error converges incrementally ($e_i = 0$). In other words, we choose the appropriate α_1 and α_2, and the observer converges exponentially when ε is sufficiently small and positive.*

The proofs of all theorems will be provided in Appendix.

4. Design of Robust Super-Twisting Sliding Mode Controller

As we all know, the trajectory tracking problem of mobile robots can be regarded as the problem of target convergence. That is tantamount to designing a suitable control strategy so that the mobile robot gradually approaches the target point driven by the control output. For this reason, this section will design an improved adaptive super-twisting sliding mode trajectory tracking controller for mobile robots.

Assume that the desired position is $q_d = \begin{bmatrix} x_d & y_d & \theta_d \end{bmatrix}^T$. We can define the position tracking error as $\varepsilon_p = q_d - q_p$. The velocity tracking error can be obtained by differentiation: $\varepsilon_v = \dot{q}_d - \dot{q}_p = \dot{q}_d - q_v$. Thus, the state-space equation of the tracking error can be expressed as

$$\begin{bmatrix} \dot{\varepsilon}_p \\ \dot{\varepsilon}_v \end{bmatrix} = \begin{bmatrix} \varepsilon_v \\ \ddot{x}_d - f(q_v) - G(\tau+\delta) \end{bmatrix}. \tag{12}$$

In order to design a super-twisting algorithm to solve the trajectory tracking problem, the sliding mode surface is defined as follows:

$$s_i = c_i\varepsilon_{pi} + \varepsilon_{vi}, \tag{13}$$

where $c_i > 0$ is a positive constant.

Since the speed information of the mobile robot is difficult to measure directly, the estimated value of the high-gain observer is used instead. Therefore, s_i can be rewritten as

$$\hat{s}_i = c_i\varepsilon_{pi} + \hat{\varepsilon}_{vi}. \tag{14}$$

Differentiation of formula (14) can be obtained as follows:

$$\begin{aligned} \dot{s}_i &= c_i\dot{\varepsilon}_{pi} + \dot{\hat{\varepsilon}}_{vi} \\ &= c_i\hat{\varepsilon}_{vi} + \ddot{q}_d - \dot{q}_v \\ &= c_i\hat{\varepsilon}_{vi} + \ddot{q}_d - f(\hat{q}_{vi}) - g_i(\tau+\delta). \end{aligned} \tag{15}$$

In the design of sliding mode control system, it is necessary to design an ideal equivalent control law τ^* to determine the dynamics of the sliding surface system. Then through identification, the ideal equivalent control law is obtained; namely,

$$\dot{s}|_{\tau(t)=\tau^*(t)} = 0. \tag{16}$$

Simultaneous equations (15) and (16) are available:

$$\tau = -\frac{1}{g_i}\left[f(\hat{q}_{vi}) - c_i\hat{\varepsilon}_{vi} - \ddot{q}_d\right] - \delta. \tag{17}$$

To solve the chattering problem in sliding mode control, the discontinuous term $\tau_s = -k_{1i}|\hat{s}_i|^{(1/2)}\mathrm{sgn}(\hat{s}_i)$ needs to be introduced, that is, the super-twisting algorithm [40]. Then, the ideal equivalent control law is obtained:

$$\tau = -\frac{1}{g_i}\left[f(q_{vi}) - c_i\hat{\varepsilon}_{vi} - \ddot{q}_d - k_{1i}|\hat{s}_i|^{1/2}\mathrm{sgn}(\hat{s}_i)\right] - \delta, \tag{18}$$

where $k_{1i} > 0$ is a gain parameter. The value is $k_{1i} = 1.5(2.1\eta_i)^{(1/2)}$.

However, the disturbance term δ is unknown when the controller is designed. Therefore, it is necessary to design an auxiliary item $k_{2i}\mathrm{sgn}(\hat{s}_i)$ instead of δ to guarantee the stability of the system. Equation (18) becomes

$$\tau = -\frac{1}{g_i}\left[f(q_{vi}) - c_i\hat{\varepsilon}_{vi} - \ddot{q}_d - k_{1i}|\hat{s}_i|^{1/2}\mathrm{sgn}(\hat{s}_i)\right] - k_{2i}\mathrm{sgn}(\hat{s}_i), \tag{19}$$

where $k_{2i} > 0$ is a gain parameter and $k_{2i} = 1.1(2.1\eta_i)$.

Remark 3. To ensure system stability, implying that $k_{2i} > |\delta|$ is established at any time.

Now, to make the mobile robot system have faster convergence speed and better motion quality. It is necessary to improve the sliding mode surface (14) and call the improved sliding mode surface as double-power sliding surface, as follows:

$$\hat{s}_i = c_i\left[\varepsilon_{pi}\right]^{\beta_1} + \left[\hat{\varepsilon}_{vi}\right]^{\beta_2}, \tag{20}$$

where $0 < \beta_i < 1\,(i = 1,2)$.

In addition, it is worth noting that the mobile robot is susceptible to external interference during actual operation, which affects the trajectory tracking task. This requires that the control parameters of the mobile robot must be adjusted

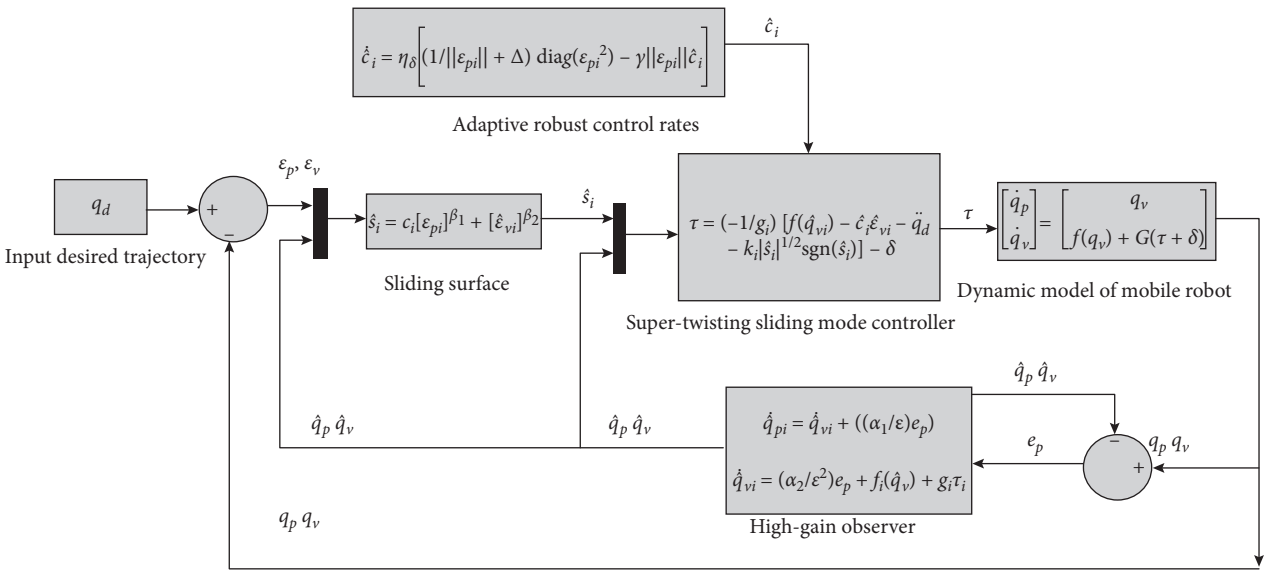

Figure 2: Block diagram of the super-twisting control based on a high-gain observer.

online in real time with the changes in the environment to make the mobile robot adaptive.

In the sliding mode surface given in equation (20), the parameter c_i is uncertain, but it can be assumed that c_i is bounded and the upper bound is known. As a consequence, the unknown control parameter c_i can be continuously and automatically estimated through the operation of robust adaptive control law, so as to continuously produce new control effects to control the controlled object, so that the controlled object follows the output of the reference model step by step until the tracking error $e(t) = 0$.

The designed robust adaptive control law is given by

$$\dot{\hat{c}}_i = \eta_\delta\left[\frac{1}{\left\|\varepsilon_{pi}\right\| + \Delta}\mathrm{diag}\left(\varepsilon_{pi}^2\right) - \gamma\left\|\varepsilon_{pi}\right\|\widehat{c}_i\right], \tag{21}$$

where η_δ and γ are positive constants and $\Delta > 0$ is a small constant called the convergence region associated with $\|\varepsilon_{pi}\|$, which prevents $\|\varepsilon_{pi}\|$ from approaching zero and causing system chattering.

Consequently, equation (21) can be rewritten as follows, and the final improved control law can be obtained from equations (18) and (21):

$$\tau = -\frac{1}{g_i}\left[f\left(\widehat{q}_{vi}\right) - \widehat{c}_i\widehat{\varepsilon}_{vi} - \ddot{q}_d - k_{1i}\left|\widehat{s}_i\right|^{(1/2)}\mathrm{sgn}\left(\widehat{s}_i\right)\right] - k_{2i}\mathrm{sgn}\left(\widehat{s}_i\right). \tag{22}$$

Finally, the input torque can be converted into the input voltage of the motor by the following formula:

$$U = \frac{R_a}{k_a r_e}E^+R^{-1}(\theta)\tau. \tag{23}$$

Theorem 2. *Based on Assumption 2, consider the dynamic robot system represented by (2). If the controller is designed as in (22), and the adaptation law is designed as in (21), then finally uniformly stable closed-loop system can be guaranteed. In addition, the tracking error ε_p can be arbitrarily reduced by adjusting the parameter γ.*

Table 1: Related parameters.

Symbol	Value
k_1, k_2	2.42
k_3	7.19
k_{11}, k_{12}	1.7
k_{13}	10.22
k_{21}, k_{22}	1.42
k_{23}	51.11
α_1	2
α_2	1
ε	0.05
β_1, β_2	0.6
γ	0.0001
Δ	0.001
η_δ	100
m_1	7 kg
m_2	0.4 kg
J_3	4.69×10^{-4} kg · m^2
r_e	64
R_a	1.9 Ω
k_a	0.013 Nm/A
k_b	0.0133 Vs/rad
k_v	0.001 Nm · s/rad
r	0.05 m
l_1	0.22 m
l_2	0.35 m
J_m	5.7×10^{-7} kg · m^2

5. Simulation Results and Discussion

To demonstrate the advantages of the improved algorithm, the simulation results are assessed. In this paper, four simulation comparisons are carried out with the same mobile robot model. The methods being compared are the conventional PID control, the super-twisting sliding mode

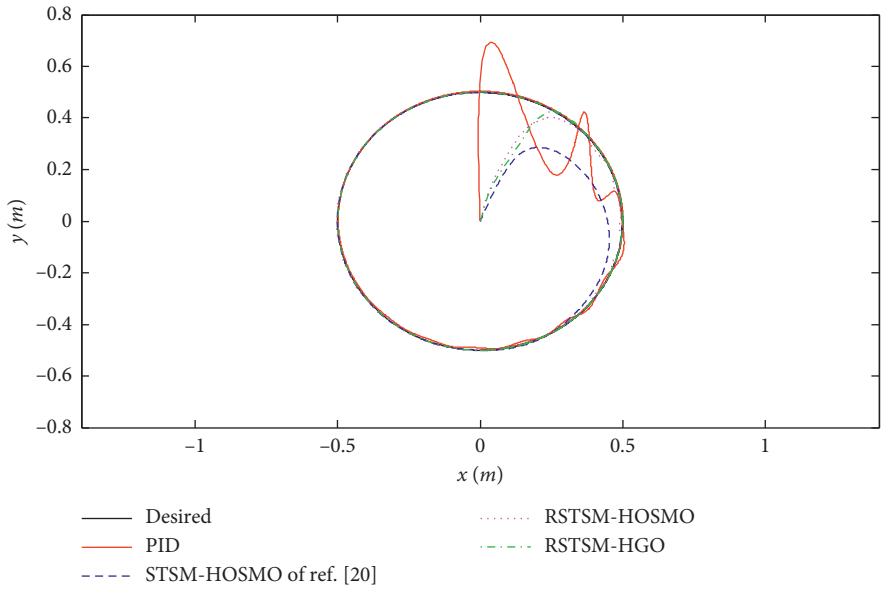

Figure 3: Circular reference trajectory tracking response diagram.

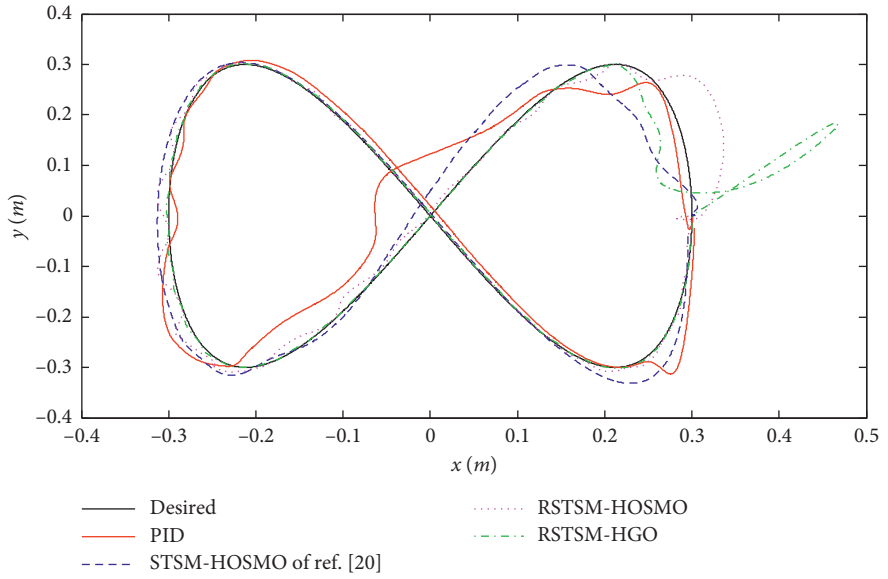

Figure 4: Eight-shaped reference trajectory tracking response diagram.

high-order observer control method (STSM-HOSMO) given in [20], the robust super-twisting sliding mode high-order observer control method (RSTSM-HOSMO), and the robust super-twisting sliding mode high-gain observer control method (RSTSM-HGO) proposed in this paper, for which the control block diagram is shown in Figure 2.

The related parameters are given in Table 1.

The PID controller is given by

$$v_i = -k_{pi}\varepsilon_{pi} - k_{di}\widehat{\varepsilon}_{vi} - k_{Ii}\int_0^1 \varepsilon_{pi}(\tau)\mathrm{d}\tau. \tag{24}$$

The gains are given as $k_{p1} = k_{p2} = 13$, $k_{p3} = 50$, $k_{d1} = k_{d2} = 1$, $k_{d3} = 5$, $k_{I1} = k_{I2} = 1.75$, and $k_{I3} = 0.75$.

The desired tracking trajectory of the set mobile robot is

$$\begin{cases} x_d = 0.5\sin(\omega t)\,(\text{units: m}), \\ y_d = 0.5\cos(\omega t)\,(\text{units: m}), \\ \theta_d = -\left(\omega t + \dfrac{\pi}{2}\right)(\text{units: rad}), \\ \omega = \dfrac{\pi}{10}\left(\text{units: } \dfrac{\text{rad}}{\text{seg}}\right). \end{cases} \tag{25}$$

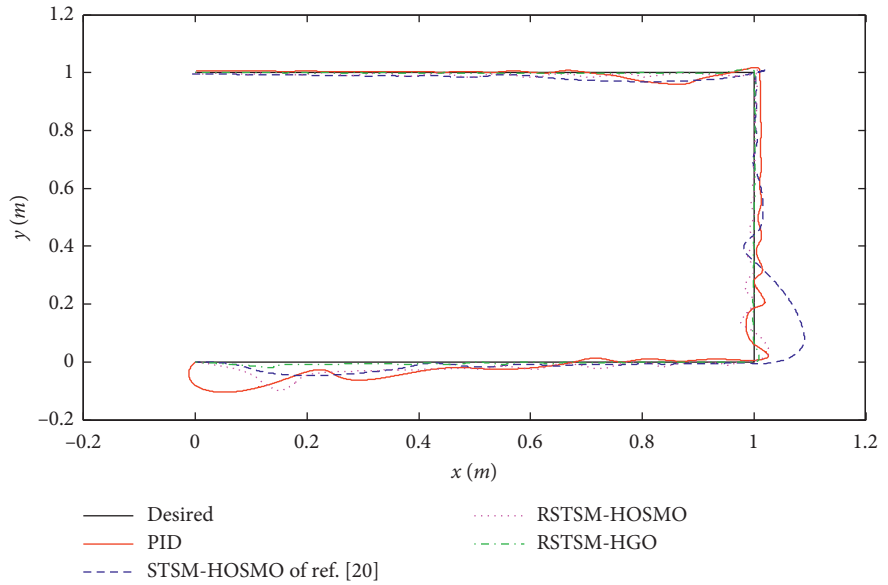

Figure 5: Anti-C-shaped reference trajectory tracking response diagram.

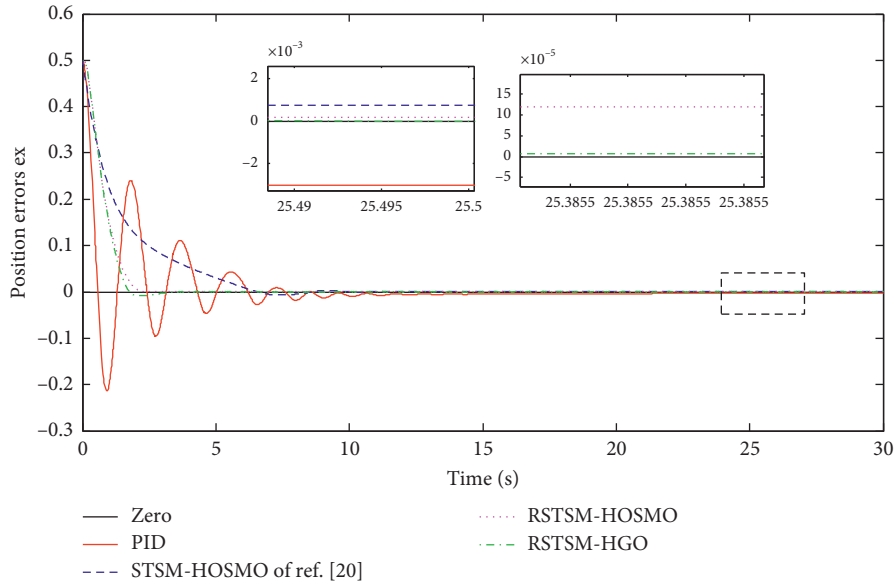

Figure 6: Trajectory tracking error.

The disturbance items are set to

$$\delta = \begin{bmatrix} \delta_1 \\ \delta_2 \\ \delta_3 \end{bmatrix} = \begin{bmatrix} 5\sin\left(\frac{\pi t}{10}\right) + 0.1 \\ -5\cos\left(\frac{\pi t}{10}\right) + 0.1 \\ 5\cos\left(\frac{\pi t}{10}\right) + 0.1 \end{bmatrix}. \quad (26)$$

The simulation results are as follows.

In the simulation verification, to verify the effectiveness of the designed control algorithm for different tracking paths, this paper traces three kinds of trajectories: respectively, circular trajectory, eight-shaped trajectory, and anti-C shaped trajectory. The tracking response is illustrated in Figures 3–5. From the three trajectory tracking effect diagrams, we can draw the conclusion that the control algorithm designed in this paper (RSTSM-HGO) has strong robustness for different reference trajectories. It benefits from the addition of adaptive law, which enables the autonomous mobile robot system to adjust the parameters in real time according to the changes in external environment. Because the PID method and the STSM-HOSMO method lack the ability to adjust online parameters, they have poorer tracking effect on the other two desired trajectories and even deviate from the desired trajectory. Only when the desired trajectory is circular, they have a good tracking effect.

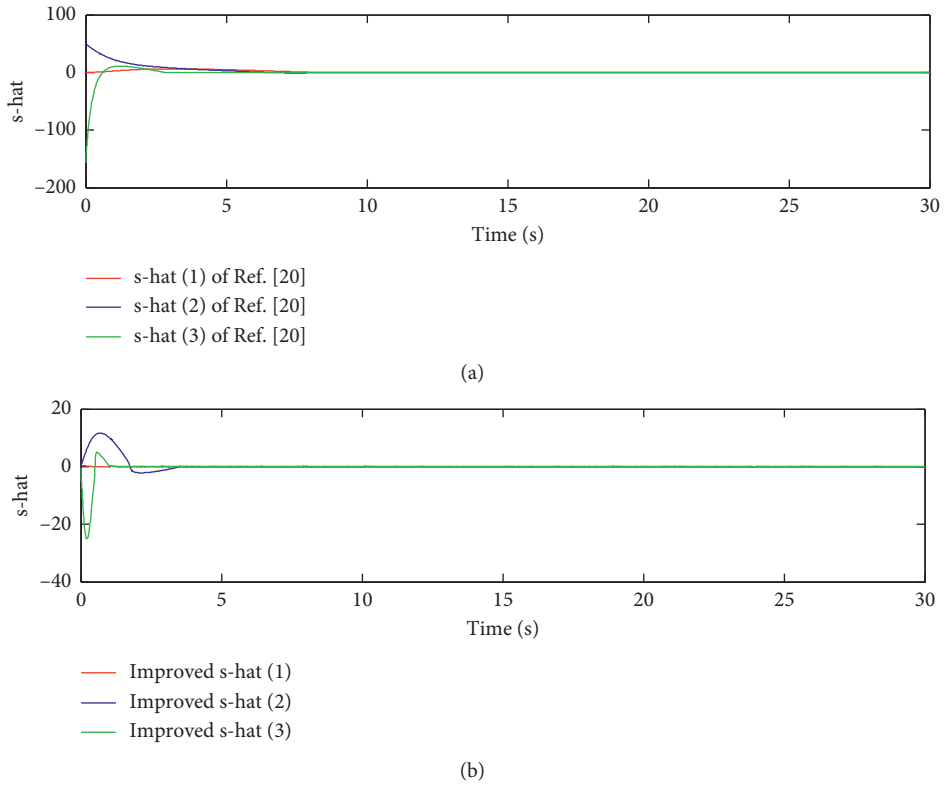

Figure 7: The sliding surface of [20] and the improved sliding surface of this paper.

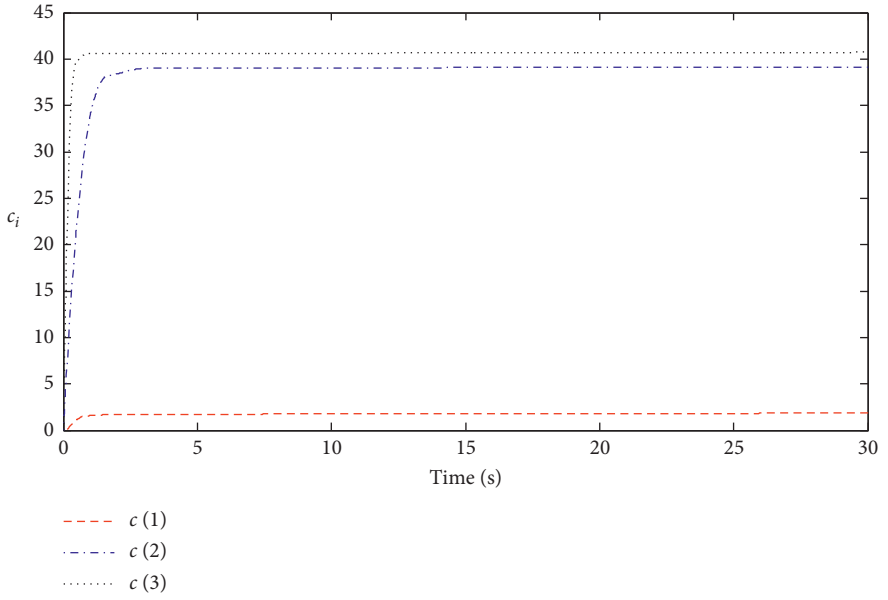

Figure 8: The output of the robust adaptive strategy.

In the following, a further analysis of the circular reference trajectory will be carried out. The simulation results in Figure 6 show that the PID controller has the fastest response speed, but the adjustment time to steady-state is the longest. However, compared with the STSM-HOSMO algorithm proposed in [20], the response speed of the RSTSM-HOSMO controller and the RSTSM-HGO controller is faster than that of the STSM-HOSMO algorithm. The appearance of such consequences just verified the conclusion that the improved super-twisting sliding mode control in this paper can effectively improve the response speed of the system. In terms of trajectory tracking accuracy, the STSM-HOSMO controller is

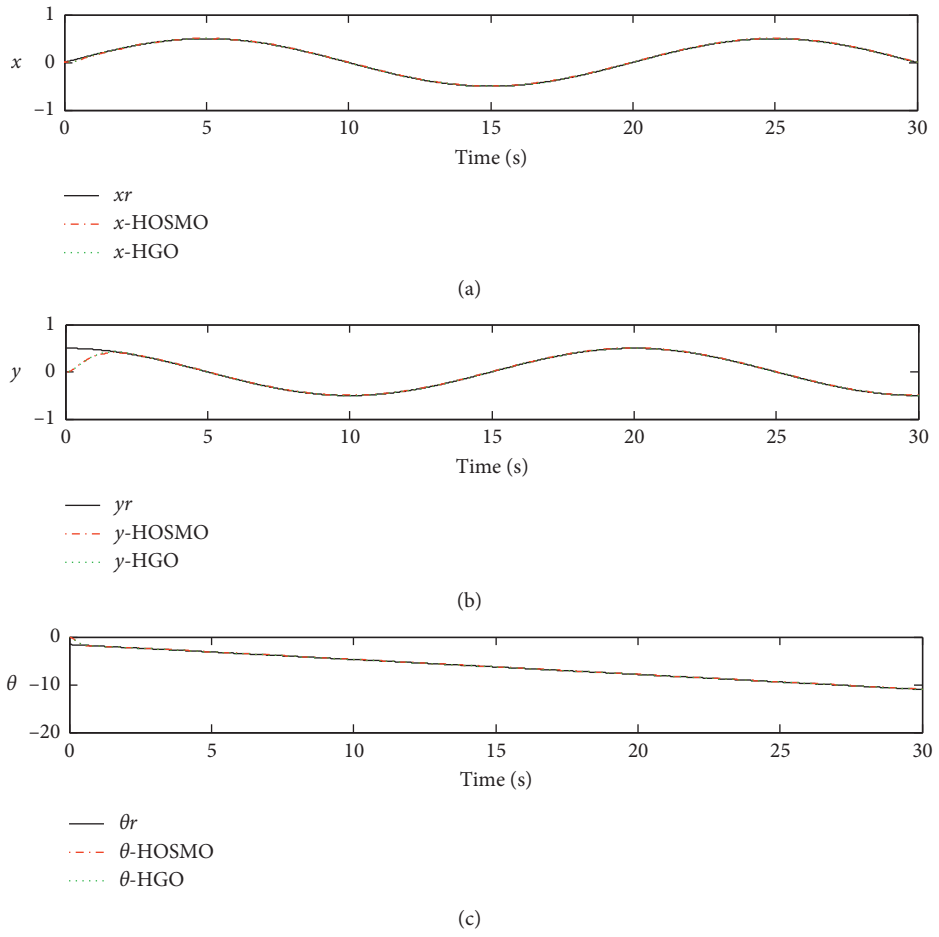

Figure 9: Comparison chart of two observers, respectively, estimating pose signals.

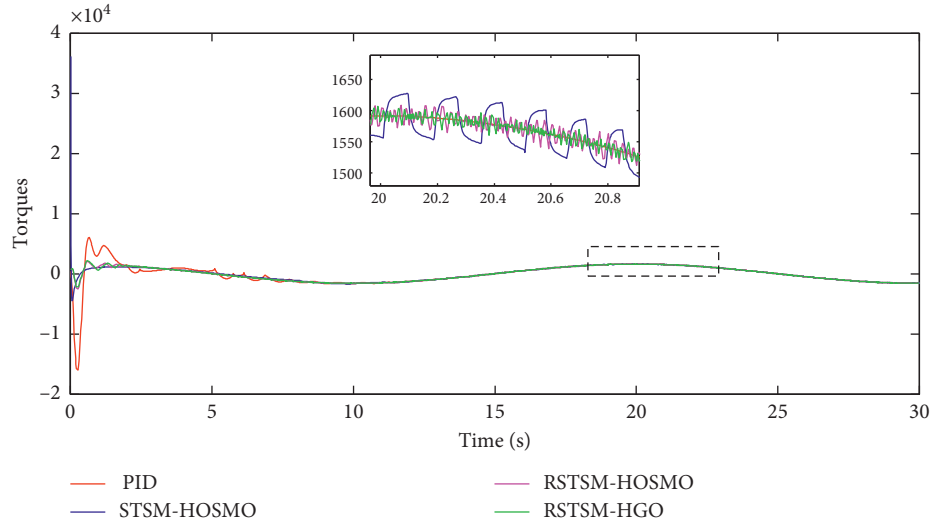

Figure 10: Temporal evolution of the control inputs.

slightly better than the PID controller with a control accuracy of approximately 10^{-3} m. The RSTSM-HGO controller is slightly better than the RSTSM-HOSMO controller. The RSTSM-HOSMO control accuracy is approximately 10^{-5} m, and the RSTSM-HGO controller accuracy is approximately 10^{-6} m, which is a very gratifying accuracy level.

Figure 7 demonstrates that although there is slight chattering after the improvement of the sliding mode

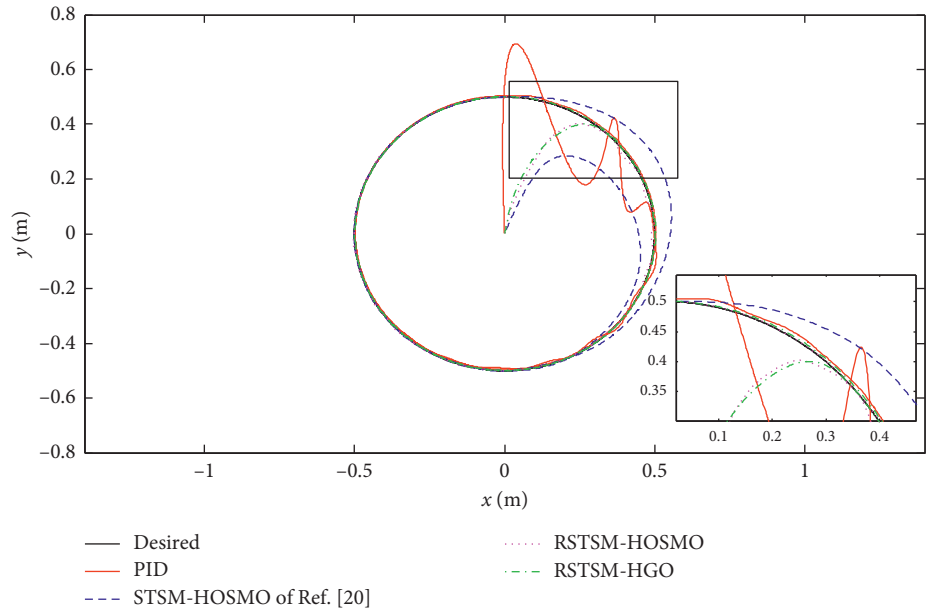

Figure 11: Circular reference trajectory tracking response diagram with disturbance.

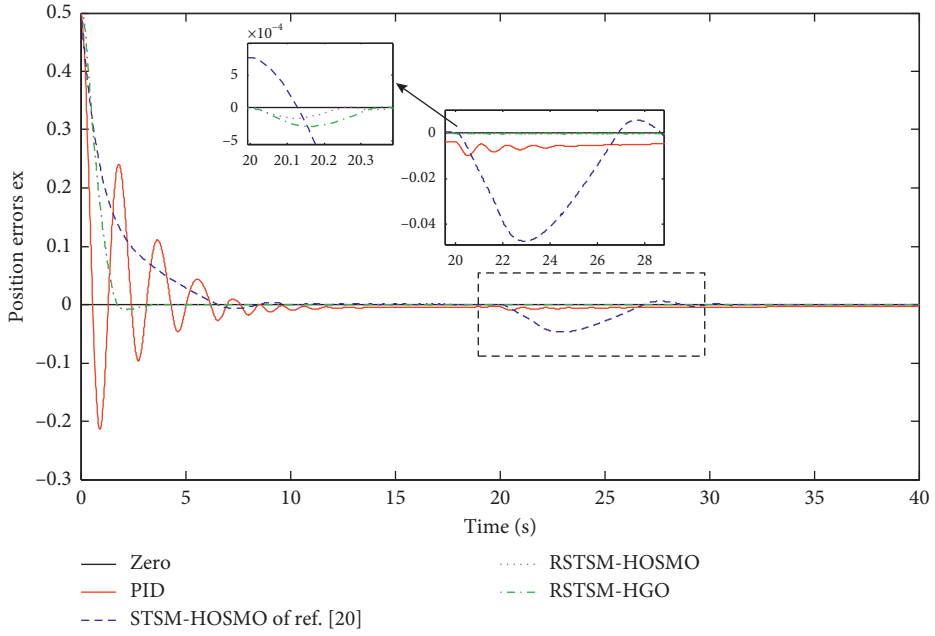

Figure 12: Trajectory tracking error with disturbance.

surface, the convergence speed of the system is accelerated. Figure 8 shows that the robust adaptive control law estimates the value of the uncertainty parameter in real time, and the value finally converges to a certain value in a bounded manner. The conclusion from Figure 9 is that both observers can effectively estimate the pose signal of the mobile robot in real time. However, since the high-gain observer has a simple structure and it is easier to program, compared with the high-order observer, the high-gain observer used in this paper is more beneficial to achieve the system's output feedback control. As shown in Figure 10, with the addition of robust adaptive control, the adjustment frequency of the system is meticulous, which makes it easier to explain why the control accuracy has improved.

To further verify the robustness of the control strategy designed in this paper, in 20 seconds, we suddenly added a 50 kg load disturbance to the mobile robot system, and the simulation results are shown in Figures 11–13.

It can be observed in Figures 11 and 12 that the control method of STSM-HOSMO is the most susceptible to disturbance after adding heavy load disturbance in 20 seconds. The PID control method is next. Under the same

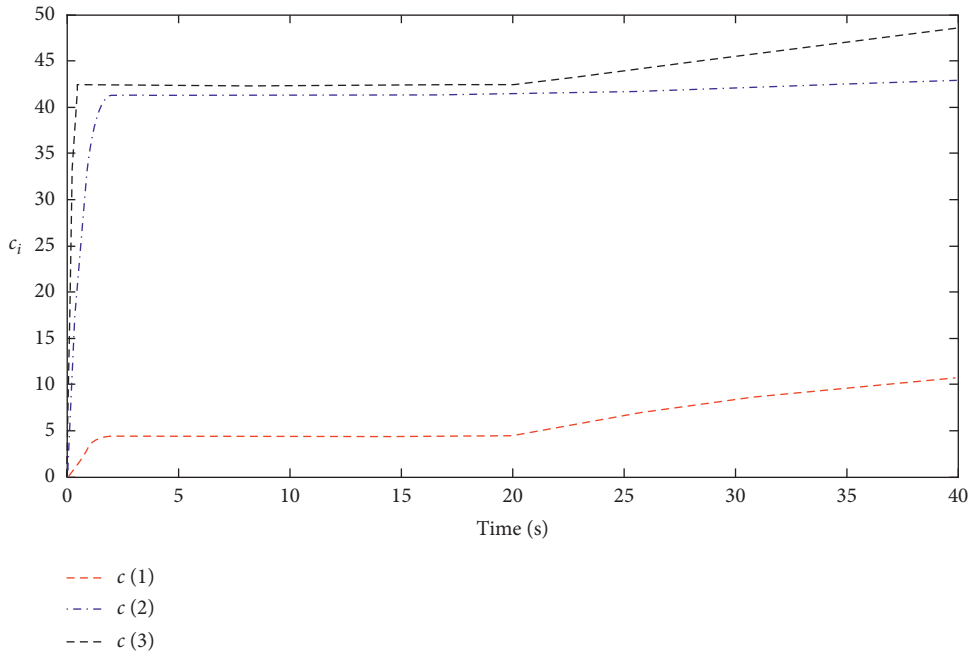

Figure 13: The output of the robust adaptive strategy with disturbance.

disturbance, only the RSTSM-HOSMO and RSTSM- HGO control methods show strong robustness to sudden disturbances, so that the tracking accuracy of the mobile robot's track tracking control does not fluctuate significantly. The reason is that the control methods of RSTSM-HOSMO and RSTSM-HGO adopt robust adaptive law to estimate the uncertainty parameter c_i in the control process, so that the parameter c_i can be adjusted to the appropriate estimate value in time with the change in the surrounding environment (as shown in Figure 13). Therefore, even if the mobile robot system is disturbed, the mobile robot still keeps excellent track control performance.

6. Conclusions

In order to address the trajectory tracking problem of a class of mobile robots driven independently by four omnidirectional wheels, a robust adaptive super-twisting sliding mode controller is proposed, and the motion control problem of parameter uncertainty and external disturbance is solved. In this paper, a double-power sliding mode surface is designed for the super-twisting sliding mode controller, which accelerates the response speed of the robot system, and the system uncertainty is better estimated by the addition of the robust adaptive controller, which makes the system more robust to uncertain factors such as external disturbances. By comparing the high-gain observer with the high-order observer, we find that the high-gain observer used throughout this paper makes the trajectory tracking control have better stability and accuracy in the implementation of output feedback control. The stability of the system is demonstrated by using the Lyapunov theory. The simulation results also verify the effectiveness of the proposed control strategy.

Appendix

Proof of Theorem 1. Define the scalar estimation error as follows:

$$\chi_1 = \frac{e_p}{\varepsilon}, \qquad \chi_2 = e_v. \tag{A.1}$$

Then, $\chi = \mathrm{col}(\chi_1, \chi_2)$ satisfies the following equation:

$$\varepsilon\dot{\chi} = F\chi + \varepsilon\delta(q, \tilde{q}, u), \tag{A.2}$$

where $F = \begin{bmatrix} -\alpha_1 & 1 \\ -\alpha_2 & 0 \end{bmatrix}$.

Because α_1 and α_2 are normal numbers, the matrix F is Hurwitz. Therefore, the eigenvalues A_0 are $1/\varepsilon$ times the F eigenvalues.

By formula (9), we know

$$|\delta| \le L\|\tilde{q}\| + M \le L\|\chi\| + M. \tag{A.3}$$

Therefore, we choose the Lyapunov function as the solution of the equation $V = \chi^T P\chi$, where P is the solution of the equation $PF + F^T P = -I$. Then, we have

$$\begin{aligned} \varepsilon\dot{V} &= -\chi^T\chi + 2\varepsilon\chi^T P\delta \\ &\le -\|\chi\|^2 + 2\varepsilon L\|P\|\|\chi\|^2 + 2\varepsilon M\|P\|\|\chi\|. \end{aligned} \tag{A.4}$$

Choose $\varepsilon L\|P\| \le 1/4$; then,

$$\varepsilon\dot{V} \le -\frac{1}{2}\|\chi\|^2 + 2\varepsilon M\|P\|\|\varepsilon\| \le -\frac{1}{4}\|\chi\|^2, \quad \forall\|\chi\| \ge 8\varepsilon M\|P\|. \tag{A.5}$$

The following conclusion is drawn in accordance with Theorem 4.5 in the book *Nonlinear Control* by Khalil [27]: $\|\chi\|$ and the corresponding $\|\tilde{q}\|$ are ultimately bounded. In other words, there are normal numbers $a, k, c < 0$, so that the following formula holds:

$$\|\chi(t)\| \le \max\left\{ke^{-(at/\varepsilon)}\|\chi(0)\|, \varepsilon cM\right\}. \tag{A.6}$$

Therefore, $\chi(t)$ shows an exponential velocity close to the ultimate boundary εcM; that is, the observer converges exponentially. This completes the proof. □

Proof of Theorem 2. Choose a positive candidate Lyapunov function as

$$V_1 = \frac{1}{2}\varepsilon_{vi}^T\varepsilon_{vi} + \eta_\delta^{-1}\left(\tilde{c}_i^T\tilde{c}_i\right). \tag{A.7}$$

The derivation of (A.7) and the substitution of (12) can be obtained:

$$\begin{aligned}\dot{V}_1 &= \varepsilon_{vi}^T\dot{\varepsilon}_{vi} + \eta_\delta^{-1}\left(\tilde{c}_i^T\dot{\tilde{c}}_i\right)\\ &= \varepsilon_{vi}^T\left[\ddot{q}_d - f(q_{vi}) - g_i(\tau+\delta)\right] + \eta_\delta^{-1}\left(\tilde{c}_i^T\dot{\tilde{c}}_i\right).\end{aligned} \tag{A.8}$$

Substituting equation (22) into equation (A.8), it becomes

$$\begin{aligned}\dot{V}_1 = \varepsilon_{vi}^T\Big[&-\hat{c}_i\hat{\varepsilon}_{vi} - k_{1i}\left|\hat{s}_i\right|^{(1/2)}\operatorname{sgn}(\hat{s}_i) - k_{2i}\operatorname{sgn}(\hat{s}_i) + \delta\Big]\\ &+ \eta_\delta^{-1}\left(\tilde{c}_i^T\dot{\tilde{c}}_i\right).\end{aligned} \tag{A.9}$$

Since $k_{2i} > |\delta|$, then $\delta - k_{2i}\operatorname{sgn}(\hat{s}_i) < 0$. And it is easy to know that $\dot{\tilde{c}}_i = \dot{c}_i - \dot{\hat{c}}_i = -\dot{\hat{c}}_i$. Then, substitute formula (21) into formula (A.9):

$$\begin{aligned}\dot{V} = &-k_i\varepsilon_{vi}^T\left|\hat{s}_i\right|^{1/2}\operatorname{sgn}(\hat{s}_i) - \varepsilon_{vi}^T\hat{c}_i\varepsilon_{vi} - \frac{1}{\left\|\varepsilon_{pi}\right\|}tr\left[\tilde{c}_i^T\operatorname{diag}\varepsilon_{pi}^T\right]\\ &+ \gamma\left\|\varepsilon_{pi}\right\|tr\left(\tilde{c}_i^T\hat{c}_i\right).\end{aligned} \tag{A.10}$$

Sinc $x^Ty = tr(yx^T)$ and $tr[\tilde{c}_i^T\operatorname{diag}(\varepsilon_{pi}^2)] = tr(\tilde{c}_i^T\varepsilon_{pi}\varepsilon_{pi}^T) = \varepsilon_{pi}^T\tilde{c}_i^T\varepsilon_{pi}$, using the Cauchy–Schwarz inequality, we have

$$\begin{aligned}\dot{V}_1 &= -\varepsilon_{vi}^T\hat{c}_i\varepsilon_{vi} - k_i\varepsilon_{vi}^T\left|\hat{s}_i\right|^{(1/2)}\operatorname{sgn}(\hat{s}_i) - \frac{1}{\left\|\varepsilon_{pi}\right\|}tr\left[\tilde{c}_i^T\operatorname{diag}\varepsilon_{pi}^T\right] + \gamma\left\|\varepsilon_{pi}\right\|tr\left(\tilde{c}_i^T\hat{c}_i\right)\\ &= -\varepsilon_{vi}^T\hat{c}_i\varepsilon_{vi} - k_i\varepsilon_{vi}^T\left|\hat{s}_i\right|^{(1/2)}\operatorname{sgn}(\hat{s}_i) - \frac{1}{\left\|\varepsilon_{pi}\right\|}\varepsilon_{pi}^T\tilde{c}_i^T\varepsilon_{pi} + \gamma\left\|\varepsilon_{pi}\right\|\left[tr\left(\tilde{c}_i^Tc_i^T\right) - \left\|\tilde{c}_i^T\right\|_F^2\right]\\ &\le -\varepsilon_{vi}^T\hat{c}_i\varepsilon_{vi} - k_i\varepsilon_{vi}^T\left|\hat{s}_i\right|^{(1/2)}\operatorname{sgn}(\hat{s}_i) - \left\|\varepsilon_{pi}\right\|\tilde{c}_i^T + \gamma\left\|\varepsilon_{pi}\right\|\left\|\tilde{c}_i^T\right\|_F\left(c_i - \left\|\tilde{c}_i^T\right\|_F\right)\\ &\le -\varepsilon_{vi}^T\hat{c}_i\varepsilon_{vi} - k_i\varepsilon_{vi}^T\left|\hat{s}_i\right|^{(1/2)}\operatorname{sgn}(\hat{s}_i) - \left\|\varepsilon_{pi}\right\|\tilde{c}_i^T - \gamma\left\|\varepsilon_{pi}\right\|\left\|\tilde{c}_i^T\right\|_F^2 + \gamma\left\|\varepsilon_{pi}\right\|\left\|\tilde{c}_i^T\right\|_Fc_i\\ &\le -\varepsilon_{vi}^T\hat{c}_i\varepsilon_{vi} - k_i\varepsilon_{vi}^T\left|\hat{s}_i\right|^{(1/2)}\operatorname{sgn}(\hat{s}_i) - \left\|\varepsilon_{pi}\right\|\tilde{c}_i^T - \gamma\left\|\varepsilon_{pi}\right\|\left\|\tilde{c}_i^T\right\|_F^2 + \gamma\left\|\varepsilon_{pi}\right\|\frac{1}{2}\left(\left\|\tilde{c}_i^T\right\|_F^2 + c_i^2\right)\\ &= -\varepsilon_{vi}^T\hat{c}_i\varepsilon_{vi} - k_i\varepsilon_{vi}^T\left|\hat{s}_i\right|^{(1/2)}\operatorname{sgn}(\hat{s}_i) - \left\|\varepsilon_{pi}\right\|\tilde{c}_i^T - \frac{1}{2}\gamma\left\|\varepsilon_{pi}\right\|\left\|\tilde{c}_i^T\right\|_F^2 + \frac{1}{2}\gamma\left\|\varepsilon_{pi}\right\|c_i^2\\ &\le -\varepsilon_{vi}^T\hat{c}_i\varepsilon_{vi} - \frac{1}{2}\gamma\left\|\varepsilon_{pi}\right\|\left\|\tilde{c}_i^T\right\|_F^2 + \frac{1}{2}\gamma\left\|\varepsilon_{pi}\right\|c_i^2\\ &\le -\mu V_1 + \sigma,\end{aligned} \tag{A.11}$$

where $\mu = \min\left\{2\hat{c}_i, \gamma\|\varepsilon_{pi}\|\eta_\delta\right\}$ and $\sigma = 1/2\gamma\|\varepsilon_{pi}\|c_i^2$.

Then, according to the generalization of the standard Lyapunov's stability theorem, the closed-loop system is uniformly ultimately bounded. This completes the proof. □

Data Availability

Data are not made available as the funding agency does not allow data sharing of the experimental program and this involves intellectual property issues.

Conflicts of Interest

The authors declare that they have no conflicts of interest.

Acknowledgments

This work was supported by the Natural Science Foundation of Guangdong Province in China (Grant no. 2018A0303130076), the Science and Technology Planning Project of Zhanjiang City (Grant no. 2017A02025), the Fostering Plan for Major Scientific Research Projects of the

Education Department of Guangdong Province-Characteristic Innovation Projects (Grant no. 2017KTSCX087), the 2019 "Chong First-Class" Provincial Financial Special Funds Construction Project (Grant no. 231419019), and the Guangdong Science and Technology Project (Grant no. 2013B011304009).

References

[1] D. Huang, J. Zhai, W. Ai, and S. Fei, "Disturbance observer-based robust control for trajectory tracking of wheeled mobile robots," *Neurocomputing*, vol. 198, pp. 74–79, 2016.

[2] E. I. A. Khatib, W. M. F. Al-Masri, S. Mukhopadhyay et al., "A comparison of adaptive trajectory tracking controllers for wheeled mobile robots," in *Proceedings of the 10th International Symposium on 2015 Mechatronics and its Applications (ISMA)*, Sharjah, UAE, December 2015.

[3] L. Xin, Q. Wang, J. She, and Y. Li, "Robust adaptive tracking control of wheeled mobile robot," *Robotics and Autonomous Systems*, vol. 78, pp. 36–48, 2016.

[4] I. Matraji, A. Al-Durra, A. Haryono, K. Al-Wahedi, and M. Abou-Khousa, "Trajectory tracking control of skid-steered mobile robot based on adaptive second order sliding mode control," *Control Engineering Practice*, vol. 72, pp. 167–176, 2018.

[5] A. Bessas, A. Benalia, and F. Boudjema, "Integral sliding mode control for trajectory tracking of wheeled mobile robot in presence of uncertainties," *Journal of Control Science & Engineering*, vol. 2016, Article ID 7915375, 10 pages, 2016.

[6] I. Salgado, D. Cruz-Ortiz, O. Camacho, and I. Chairez, "Output feedback control of a skid-steered mobile robot based on the super-twisting algorithm," *Control Engineering Practice*, vol. 58, pp. 193–203, 2017.

[7] Y. Shtessel, M. Taleb, and F. Plestan, "A novel adaptive-gain supertwisting sliding mode controller: methodology and application," *Automatica*, vol. 48, no. 5, pp. 759–769, 2012.

[8] M. Boukens and A. Boukabou, "Design of an intelligent optimal neural network-based tracking controller for non-holonomic mobile robot systems," *Neurocomputing*, vol. 226, pp. 46–57, 2017.

[9] X. Jin, "Fault-tolerant iterative learning control for mobile robots non-repetitive trajectory tracking with output constraints," *Automatica*, vol. 94, pp. 63–71, 2018.

[10] S. Li, L. Ding, H. Gao, C. Chen, Z. Liu, and Z. Deng, "Adaptive neural network tracking control-based reinforcement learning for wheeled mobile robots with skidding and slipping," *Neurocomputing*, vol. 283, pp. 20–30, 2018.

[11] J.-J. Slotine, W. Li, and P. Hall, *Applied Nonlinear Control: United States*, Pearson Schweiz Ag, Zug, Switzerland, 1990.

[12] J. A. Burton and A. S. I. Zinober, "Continuous approximation of variable structure control," *International Journal of Systems Science*, vol. 17, no. 6, pp. 875–885, 1986.

[13] L. Amet, M. Ghanes, and J.-P. Barbot, "HOSM control under quantization and saturation constraints: zig-Zag design solutions," in *Proceedings of the IEEE IEEE Conference on Decision & Control*, pp. 5494–5498, Maui, HI, USA, December 2013.

[14] H. M. Becerra, J. A. Colunga, and J. G. Romero, "Robust trajectory tracking controllers for pose-regulation of wheeled mobile robots," in *Proceedings of the 2016 IEEE/RSJ International Conference on Intelligent Robots and Systems, IROS 2016*, pp. 1041–1047, Institute of Electrical and Electronics Engineers Inc., Daejeon, Republic of Korea, October 2016.

[15] E. El'Youssed, N. A. Martins, E. R. D. Pieri et al., "PD-Super-Twisting second order sliding mode tracking control for a nonholonomic wheeled mobile robot," *IFAC Proceedings Volumes*, vol. 45, no. 22, pp. 429–434, 2012.

[16] S. Ankalaki, S. C. Gupta, B. P. Prasath et al., "Design and implementation of neural network based non linear control system (LQR) for target tracking mobile robots," in *Proceedings of the International Conference on Advances in Computing*, Bangalore, India, September 2018.

[17] M. Boukens, A. Boukabou, and M. Chadli, "Robust adaptive neural network-based trajectory tracking control approach for nonholonomic electrically driven mobile robots," *Robotics and Autonomous Systems*, vol. 92, pp. 30–40, 2017.

[18] X. Wu, P. Jin, T. Zou et al., "Backstepping trajectory tracking based on fuzzy sliding mode control for differential mobile robots," *Journal of Intelligent & Robotic Systems*, vol. 96, no. 1, pp. 109–121, 2019.

[19] H.-M. Wu and M. Karkoub, "Hierarchical fuzzy sliding-mode adaptive control for the trajectory tracking of differential-driven mobile robots," *International Journal of Fuzzy Systems*, vol. 21, no. 1, pp. 33–49, 2019.

[20] L. Ovalle, H. Ríos, M. Llama, V. Santibáñez, and A. Dzul, "Omnidirectional mobile robot robust tracking: sliding-mode output-based control approaches," *Control Engineering Practice*, vol. 85, pp. 50–58, 2019.

[21] S. Keshtkar and A. Poznyak, "Adaptive sliding mode controller based on super-twist observer for tethered satellite system," *International Journal of Control*, vol. 89, no. 9, pp. 1904–1915, 2016.

[22] H. K. Khalil and L. Praly, "High-gain observers in nonlinear feedback control," *International Journal of Robust and Nonlinear Control*, vol. 24, no. 6, pp. 993–1015, 2014.

[23] H. Liu and H. K. Khalil, "Output feedback stabilization using super-twisting control and high-gain observer," *International Journal Of Robust And Nonlinear Control*, vol. 29, no. 3, pp. 601–617, 2019.

[24] A. Chalanga, "Implementation of super-twisting control on higher order perturbed integrator system using higher order sliding mode observer," *IEEE Transactions on Industrial Electronics*, vol. 49, no. 18, pp. 873–878, 2016.

[25] A. Daniele, "Stubborn ISS redesign for nonlinear high-gain observers," *IFAC PapersOnline*, vol. 50, no. 1, pp. 15422–15427, 2017.

[26] H. K. Khalil, "Cascade high-gain observers in output feedback control," *Automatica*, vol. 80, pp. 110–118, 2017.

[27] H. K. Khalil, *Nonlinear Control: Chinese Translation Version*, pp. 61–63, Mechanical Industry Publishing, Beijing, China, 2016.